Supporting Information

Lorieau et al. 10.1073/pnas.1006142107

SI Text

SI Materials and Methods ***Sample preparation.*** HAfp$^{1-23}$ of sero type H1 was expressed as a fusion protein, flanked by the residues SGKKKKD at its C terminus and by the Igg-binding domain B1 of streptococcal protein G (GB1; PDB entry 3GB1) at its N terminus. The GB1 domain encompasses a His-tag and a factor Xa protease (FXa) cleavage site at its N and C termini, respectively. The sequence of the final purified peptide is GLFGAIAGFI EGGWTGMIDG WYGSGKKKKD. Standard growth conditions were used for the expression and isotope labeling of the fusion protein (1). It was isolated under denaturing conditions using Ni-NTA affinity chromatography, dialyzed against FXa buffer and subjected to FXa cleavage. The digest was passed over another Ni-NTA column and the flow-through was concentrated and subjected to size-exclusion chromatography on Superdex-75. Integrity of HAfp-K4D was verified by mass spectrometry.

NMR samples were prepared to final concentrations of ca 0.6 mM HAfp$^{1-23}$ in 130–180 mM protonated or perdeuterated (for measurement of two-dimensional NOESY spectra) DPC (Anatrace), in 93%H_2O/7%D_2O or 99.9% D_2O (for measurement of two-dimensional NOESY spectra), containing 1X protease inhibitor cocktail (Roche Diagnostics), 25 mM ^{2}H-Tris at pH 7.4 (Cambridge Isotopes) or a mixture of 20 mM ^{2}H-Tris and 7 mM ^{2}H-citric acid (Cambridge Isotopes) at pH 4.0. The ^{15}N- and ^{13}C, ^{15}N-labeled fusion peptide samples were also prepared in >99% ^2H_2O, by lyophilizing 280 μL of an H_2O sample, and dissolving the powder in 100% ^2H_2O in a N_2 glove box.

Stretched acrylamide gel (SAG) samples (2, 3) for RDC measurement were prepared as described by Chou et al.(4). The SAG was negatively charged and prepared from 5.91% (w/v) acrylamide (AA)/2-(acrylamido)-2-methyl-1-propanesulfonic acid (AMPS)/bis(acrylamide) (BIS) (4.37% AA, 1.42% AMPS, 0.12% BIS), 0.1% (w/v) ammonium persulfate, and 0.1% (v/v) N, N, N' ,N'- tetramethylethylenediamine in 150 mM Tris-HCl buffer at pH 8.0. A SAG of 280 μL was cast in a 5.4 mm cylinder. The polymerized gels were soaked for 1 d in 50 mL H_2O followed by 2 d in either 50 mL of 25 mM imidazole pH 7.0 or 50 mL of 20 mM citric acid pH 4.0. The gels were dehydrated at 37 °C for 24 h, soaked in 280 μL of the fusion peptide sample (above) for 2 d, and inserted into a 4.1 mm inner diameter NMR tube using a funnel (4). The alignment was monitored by the residual quadrupolar splitting (RQC) of ^2H_2O; the initial RQC was 2.56 Hz for the pH 7.4 sample, and 3.22 Hz for the pH 4.0 sample, and the RQC decreased by <10% over the course of multiple experiments.

Samples aligned by a liquid crystalline solution of the dinucleotide d(GpG) (5) were prepared by adding 80 mM KCl (Sigma-Aldrich) and 15 mg/mL Na-d(GpG) (Rasayan Inc.) to 280 μL of the HAfp$^{1-23}$ sample (above). The RQC of the ^2H_2O signal was 16.8 Hz.

NMR data collection and analysis. Resonance assignments were made on the basis of ^{15}N-HSQC, HNCO, HNCA, constant-time ^{13}C-HSQC spectra, and HACAN, all with Rance-Kay gradient-enhanced detection schemes. Assignments were confirmed by three-dimensional HNH-NOESY-HMQC and two-dimensional NOESY experiments. The HNH^N-NOESY-HMQC experiments were conducted at 600 MHz and 900 MHz ^{1}H frequency on the ^{15}N-labeled peptide with nonselective excitation preceding the NOE mixing period and using EBurp- and ReBurp-shaped (6) H^N-selective pulses for the HMQC readout sequence following the 100 ms NOE mixing period. Two-dimensional NOESY experiments were carried out at 900 MHz on ^{15}N-labeled peptide in 99.8% ^2H_2O, using a 10 Hz water presaturating radiofrequency field between transients, and NOE mixing times of 70 and 150 ms.

Conversion of NOE intensities to distance restraints was carried out in a semiquantitative manner, which empirically accounts for spin-diffusion enhancements to intensities (7), and the exponent k of the r_{HH}^{-k} distance dependence was derived by comparing short and medium-range NOE intensities observed for residues 3–10 with interproton distances in an idealized α-helix. The covalently-fixed distances between aromatic protons of Trp-14 and Trp-21 were also added to this calibration, as were the H^α-H^β cross peak intensities of the Ala residues.

The $^1D_{NH}$, $^1D_{C\alpha H\alpha}$, $^1D_{CH3}$ and $^2D_{H\alpha1H\alpha2}$ couplings in the SAG-aligned samples were measured using two-dimensional ^{1}H-^{15}N IPAP-HSQC (8), three-dimensional ^{1}H^α-coupled HNCOCA, two-dimensional ^{1}H-coupled constant-time ^{13}C-HSQC, and two-dimensional CH_2 S^{3}E-HSQC (9) experiments, respectively. The $^1D_{CH3}$ couplings were converted to dipolar restraints for the $^1D_{CC(H3)}$ interaction (10) for structure calculation purposes. The individual $D_{C\alpha H\alpha2}$ and $D_{C\alpha H\alpha3}$ couplings for Gly^1, Gly^{12}, and Gly^{13} were derived from measurements in the two-dimensional ^{13}C-coupled CH_2 S^{3}E-HSQC experiment and used instead of the $D_{C\alpha H\alpha2} + D_{C\alpha H\alpha3}$ sum coupling. The SVD analysis of the dipolar couplings was conducted with the program DC (11).

The $^1D_{NH}$, $^1D_{NCO}$/$^2D_{HCO}$, and $^1D_{COCA}$, couplings in the dGpG-aligned sample were measured using two-dimensional ^{1}H-^{15}N IPAP-HSQC, two-dimensional ^{13}C'-coupled TROSY-HSQC, and a three-dimensional ^{13}C^α, ^{15}N-coupled HNCO, respectively.

Three-bond J-couplings ($^3J_{NC\gamma}$ and $^3J_{C'C\gamma}$) reporting on the χ_1 angles of aromatic residues were measured using 50 ms and 40 ms delta periods in the constant-time spin-echo difference two-dimensional ^{1}H-^{15}N HSQC and three-dimensional TROSY-HNCO experiments (12), respectively.

The backbone ^{15}N R_1, R_2, and {^{1}H}-^{15}N NOE relaxation values were measured at 600 MHz on the ^{15}N-labeled sample, using methods described previously (13). The relaxation parameters were analyzed using the program ModelFree (14, 15), assuming an axially symmetric ^{15}N CSA of −173 ppm applicable for α-helical amide groups (16), a librationally adjusted ^{1}H-^{15}N bond length of 1.04 Å (17), and an isotropic diffusion model. Hydrogen exchange was measured as described in (18).

Structure calculations. Structure calculations were started from a fully extended chain. Using a simulated annealing molecular dynamics program, implemented in XPLOR-NIH 2.25 (19, 20), the trajectory was started at 3,000 K and cooled down linearly to 30 K in 10 K temperature steps with the variable time step internal variable dynamics module (IVM) algorithm (21). Each temperature step was propagated for 100 simulation steps or 0.2 ps simulation time, whichever was less. A quartic repulsive nonbonded potential was used, with the atomic radii scaled from the van der Waals values multiplicatively, from 0.90 to 0.81. NOE restraint force constants were ramped multiplicatively from 0.2 to 20 kcal/Å^2, using a soft-square potential (22); Residual dipolar coupling (RDC) restraints were implemented harmonically with a force constant ramped multiplicatively from 10^{-4} to 0.25 kcal/Hz^2 for $^1D_{NH}$ couplings during the 3,000 → 30 K cool down. Force constants for $^1D_{C\alpha H\alpha}$, $^1D_{C'N}$, $^1D_{C'H}$, $^1D_{C'C\alpha}$, $^1D_{C-(CH3)}$, $^1D_{H\alpha2H\alpha3}$ were scaled relative to $^1D_{NH}$ by factors of 0.2, 26, 2.2, 4.4, 11, and 0.01, respectively.

The C^{α}H-O=C hydrogen bonds, corroborated by characteristic NOE patterns, are not parameterized by the hydrogen bond database (HBDB) empirical potential of mean force (23), and they were modeled with a half-harmonic potential ($k = 20$ kcal/mol) with $a \leq 2.7$ Å cutoff on the H^{α} to O distance (24). This potential was applied for hydrogen bonds between Phe^{9} H^{α} and Gly^{13} C=O, Ala^{5} $H^{\alpha}$and Met^{17} C=O, Met^{17} H^{α} and Ala^{5} C=O, and Trp^{21} H^{α} and Gly^{1} C=O.

A free-mode run of HBDB discovered hydrogen bonds between the protons of Gly^{1}-NH_3^+ and the carbonyl oxygens of Gly^{20} and other C-terminal residues. The Gly^{1}/Gly^{20} hydrogen bond was entered in the HBDB fixed list. Hydrogen bonds between Gly^{1}/Trp^{21} or Gly^{1}/Gly^{23}, or both, were present in a subset of structures, but inclusion of these hydrogen bonds did not improve the structural statistics, and therefore, they were not included in the final refinement. Structural statistics are listed in Table S1.

There were no persistent NOE violations above 0.25 Å, and two violations between 0.2–0.25 Å (Phe^{3}H^{α}-Phe^{3}$H^{\delta\epsilon\gamma}$ and Ile^{10}H^{α}-Ile^{10}$H^{\delta 1}$). Ile^{10} has a strong spin-diffusion pathway (*via* Ile^{10}$H^{\gamma 2}$), and the orientation of the aromatic ring of Phe^{3} is dynamically disordered (Table S2).

1. Koenig BW, Rogowski M, Louis JM (2003) A rapid method to attain isotope labeled small soluble peptides for NMR studies.*J Biomol NMR* 26:193–202.
2. Tycko R, Blanco FJ, Ishii Y (2000) Alignment of biopolymers in strained gels: a new way to create detectable dipole-dipole couplings in high-resolution biomolecular NMR. *J Am Chem Soc* 122:9340–9341.
3. Sass H.-J, Musco G, Stahl SJ, Wingfield PT, Grzesiek S (2000) Solution NMR of proteins within polyacrylamide gels: diffusional properties and residual alignment by mechanical stress or embedding of oriented purple membranes. *J Biomol NMR* 18:303–309.
4. Chou JJ, Gaemers S, Howder B, Louis JM, Bax A (2001) A simple apparatus for generating stretched polyacrylamide gels, yielding uniform alignment of proteins and detergent micelles. *J Biomol NMR* 21:377–382.
5. Lorieau J, Yao LS, Bax A (2008) Liquid crystalline phase of G-tetrad DNA for NMR study of detergent-solubilized proteins. *J Am Chem Soc* 130:7536–7537.
6. Geen H, Freeman R (1991) Band-selective radiofrequency pulses. *J Magn Reson* 93:93–141.
7. Guntert P, Braun W, Wuthrich K (1991) Efficient computation of three-dimensional protein structures in solution from nuclear-magnetic-resonance data using the program Diana and the supporting programs Caliba, Habas, and Glomsa. *J Mol Biol* 217:517–530.
8. Yao LS, Ying JF, Bax A (2009) Improved accuracy of N-15-H-1 scalar and residual dipolar couplings from gradient-enhanced IPAP-HSQC experiments on protonated proteins. *J Biomol NMR* 43:161–170.
9. Miclet E, O'Neil-Cabello E, Nikonowicz EP, Live D, Bax A (2003) H-1-H-1 dipolar couplings provide a unique probe of RNA backbone structure. *J Am Chem Soc* 125:15740–15741.
10. Ottiger M, Bax A (1999) How tetrahedral are methyl groups in proteins? A liquid crystal NMR study. *J Am Chem Soc* 121:4690-4695.
11. Delaglio F, et al. (1995) NMRpipe—a multidimensional spectral processing system based on Unix pipes. *J Biomol NMR* 6:277-293.
12. Hu JS, Grzesiek S, Bax A (1997) Two-dimensional NMR methods for determining (chi 1) angles of aromatic residues in proteins from three-bond J(C′C gamma) and J(NC gamma) couplings. *J Am Chem Soc* 119:1803–1804.
13. Farrow NA, et al. (1994) Backbone dynamics of a free and a phosphopeptide-complexed Src homology 2 domain studied by ^{15}N NMR relaxation. *Biochemistry* 33:5984–6003.
14. Mandel AM, Mikael A, Palmer AG (1995) Backbone dynamics of *Escherichia coli* Ribonuclease HI: correlations with structure and function in an active enzyme. *J Mol Biol.* 246:144–163.
15. Cole R, Loria JP (2003) FAST-Model-free: a program for rapid automated analysis of solution NMR spin-relaxation data. *J Biomol NMR* 26:203–213.
16. Yao L, Grishaev A, Cornilescu G, Bax A (2010) Site-specific backbone amide 15N chemical shift anisotropy tensors in a small protein from liquid crystal and cross-correlated relaxation measurements. *J Am Chem Soc* DOI: 10.1021/ja910186u.
17. Yao L, Voegeli B, Ying JF, Bax A (2008) NMR determination of amide N-H equilibrium bond length from concerted dipolar coupling measurements. *J Am Chem Soc* 130:16518–16520.
18. Chill JH, Louis JM, Miller C, Bax A (2006) NMR study of the tetrameric KcsA potassium channel in detergent micelles. *Protein Science* 15:684–698.
19. Schwieters CD, Kuszewski JJ, Tjandra N, Clore GM (2003) The Xplor-NIH NMR molecular structure determination package. *J Magn Reson.* 160:65–73.
20. Schwieters CD, Kuszewski JJ, Clore GM (2006) Using Xplor-NIH for NMR molecular structure determination. *Prog Nucl Mag Res Sp* 48:47–62.
21. Schwieters CD, Clore GM (2001) Internal coordinates for molecular dynamics and minimization in structure determination and refinement. *J Magn. Reson* 152:288–302.
22. Brunger AT (1993) *XPLOR Manual Version 3.1* (Yale University Press, New Haven, CT).
23. Grishaev A, Bax A (2004) An empirical backbone-backbone hydrogen-bonding potential in proteins and its applications to NMR structure refinement and validation. *J Am Chem Soc* 126:7281–7292.
24. Senes A, Ubarretxena-Belandia I, Engelman DM (2001) The C alpha-H center dot center dot center dot O hydrogen bond: a determinant of stability and specificity in transmembrane helix interactions. *Proc Nat'l Acad Sci USA* 98:9056–9061.
25. Davis IW, Murray LW, Richardson JS, Richardson DC (2004) MolProbity: structure validation and all-atom contact analysis for nucleic acids and their complexes. *Nucleic Acids Res* 32: W615–W619.
26. Cornilescu G, Marquardt JL, Ottiger M, Bax A (1998) Validation of protein structure from anisotropic carbonyl chemical shifts in a dilute liquid crystalline phase. *J Am Chem Soc* 120:6836–6837.
27. Clore GM, et al. (1999) R-factor, free R, and complete cross-validation for dipolar coupling refinement of NMR structures. *J Am Chem Soc* 121:9008–9012.
28. Laskowski RA, MacArthur MW, Moss DS, Thornton JW (1993) PROCHECK: a program to check the stereochemical quality of protein structures. *J Appl Cryst* 26:283–291.
29. Bhattacharya A, Tejero R, Montelione GT (2007) Evaluating protein structures determined by structural genomics consortia. *Proteins-Structure Function And Bioinformatics* 66:778–795.

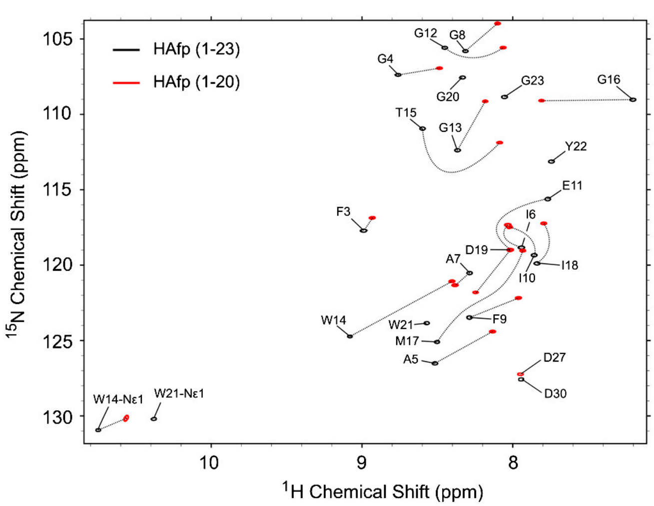

Fig. S1. Comparison of the ^{1}H-^{15}N HSQC two-dimensional spectra (600 MHz ^{1}H frequency, pH 7.4, 0.8 mM in 180 mM ^{2}H-DPC at 33 °C) of the H1 hemagglutinin fusion peptide HAfp$^{1-23}$ (black) with that of the truncated peptide HAfp$^{1-20}$ (red). Both peptides contain a C-terminal heptapeptide, consisting of SGKKKKD, to facilitate sample preparation. Resonances of the C-terminal residues (Gly^{20}-Lys^{26} in HAfp$^{1-20}$ and Ser^{24}-Lys^{29} in HAfp$^{1-23}$ are missing from the spectra due to rapid exchange with solvent).

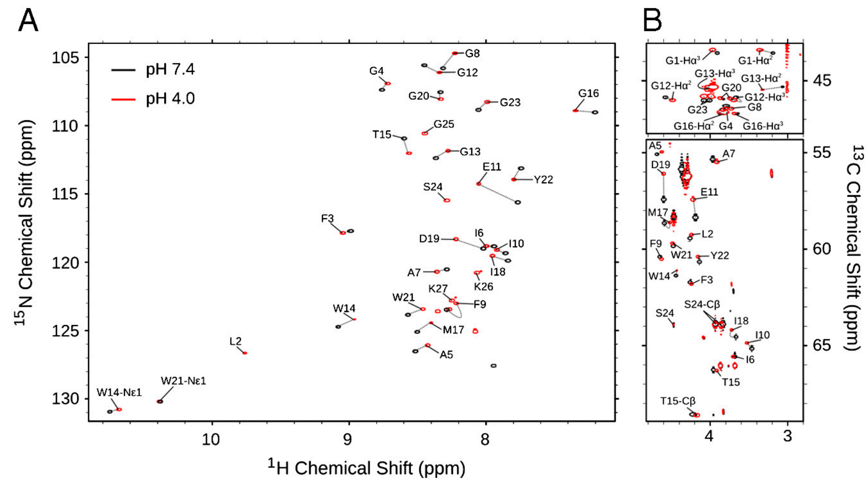

Fig. S2. Comparison of HAfp$^{1-23}$ spectra at pH 7.4 (black) and pH 4.0 (red). (*A*) ^{1}H-^{15}N HSQC spectrum and (*B*) ^{1}H-^{13}C HSQC spectrum ($^{13}C^{\alpha}$ region). Both sets of spectra were recorded at 900 MHz ^{1}H frequency, 33 °C.

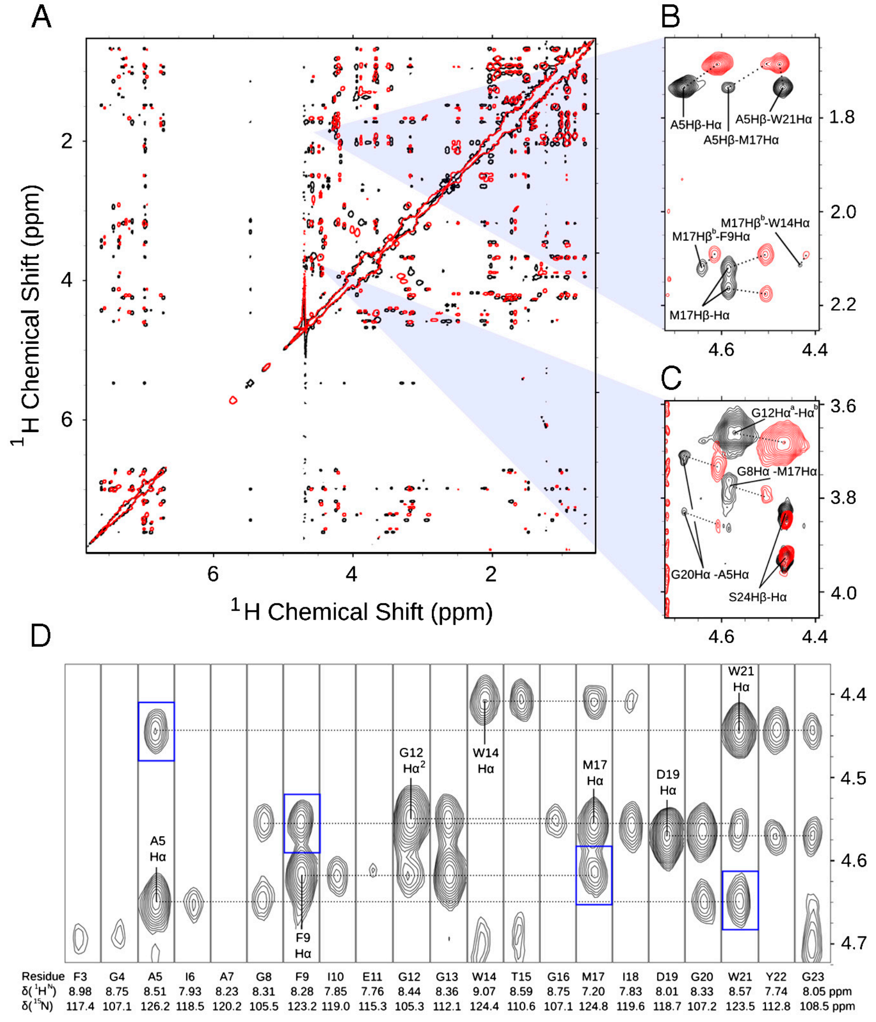

Fig. S3. Superimposed 900-MHz NOESY spectra of HAfp$^{1-23}$ at pH 7.4 (black) and pH 4.0 (red). (*A*) Two-dimensional NOESY spectrum recorded with a mixing time of 150 ms. (*B–C*) Expanded regions from two-dimensional NOESY spectra (mixing time 70 ms) highlighting interhelical $^{1}H^{\alpha}$-$^{1}H^{\beta}$ NOE connectivities between Ala^{5} and Trp^{21}, Ala^{5} and Met^{17}, Phe^{9} and Met^{17}, and $^{1}H^{\alpha}$-$^{1}H^{\alpha}$ NOE connectivities between Gly^{8} and Met^{17}, and Ala^{5} and Gly^{20}. (*D*) Strip plots taken from a three-dimensional ^{15}N-separated NOESY-HMQC spectrum, showing long-range interhelical NOE connectivities between $^{1}H^{\alpha}$ and backbone $^{1}H^{N}$ as well as the expected $d_{\alpha N}(i,i+3)$ intrahelical NOE connectivities. Strong interhelical H^{α}-H^{N} NOEs are observed when H^{α} and H^{N} share hydrogen bonds to the same backbone carbonyl oxygen. These NOEs, which include Trp$^{21}H^{\alpha}$-Ala$^{5}H^{N}$, Met$^{17}H^{\alpha}$-Phe$^{9}H^{N}$, Phe$^{9}H^{\alpha}$-Met$^{17}H^{N}$, and Ala$^{5}H^{\alpha}$-Trp$^{21}H^{N}$, are marked by blue boxes.

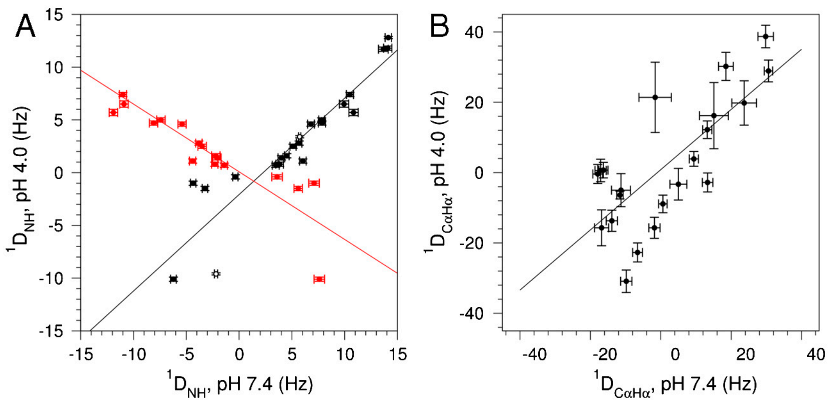

Fig. S4. Plot of backbone RDCs in HAfp$^{1-23}$ measured at low pH vs. corresponding values measured at high pH. (*A*) $^{1}D_{NH}$ couplings; (*B*) $^{1}D_{C\alpha H_\alpha}$ couplings. High pH values were measured both in liquid crystalline d(GpG) (red) and in negatively charged polyacrylamide gel (black)—see *SI Materials and Methods* section. RDCs at pH 4.0 were measured in negatively charged polyacrylamide gel only. Correlation coefficients for the fits are (*A*) 0.86 (red trace), 0.89 (black trace), and (*B*) 0.56. The low degrees of correlation reflects the different orientations of Hafp$^{1-23}$ relative to the magnetic field at high and low pH. The close anticorrelation between pH4.0 d(GpG) and polyacrylamide gel data ($R = 0.97$) indicates very similar alignment matrices, but with opposite sign, reflecting the orthogonal orientation of dGpG columns relative to the magnetic field, whereas stretched gel aligns in a parallel manner.

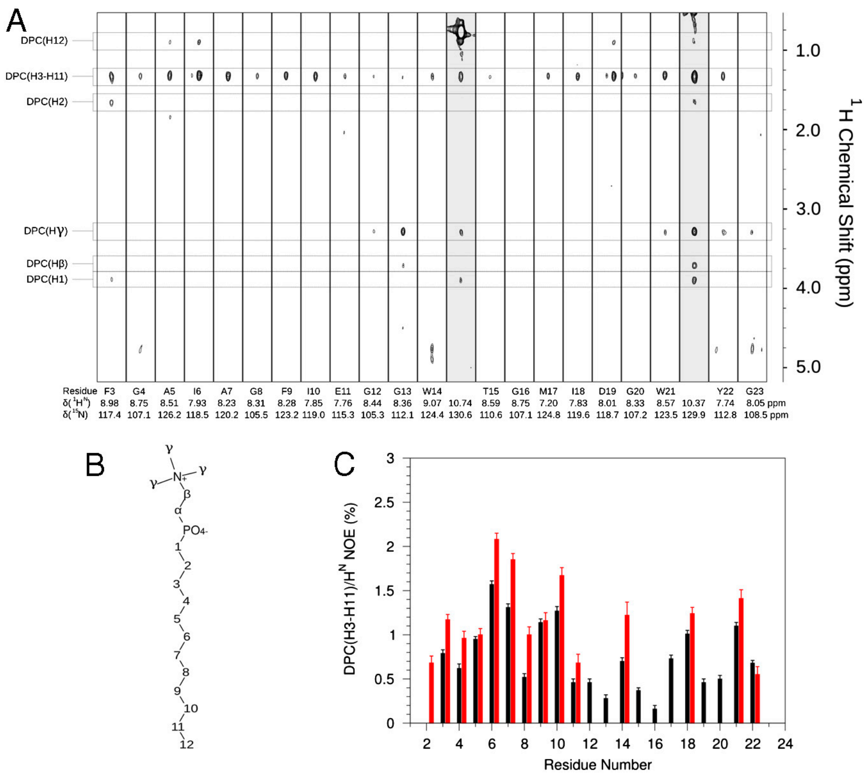

Fig. S5. Strip plots taken from the pH 7.4 three-dimensional ^{15}N-separated NOESY-HMQC spectrum (100 ms mix time) of uniformly perdeuterated HAfp$^{1-23}$ dissolved in protonated DPC, showing intermolecular NOE interactions between detergent and backbone amide protons. Strips for NOEs to the Trp H^{ε_1} protons are shaded gray. The diagonal resonance of Trp^{14}-H^{ε_1} and Trp21—H^{ε_1} are aliased and appear at 0.77 ppm and 0.43 ppm, respectively. (*B*) The DPC structure with the carbon atoms labeled by position. (*C*) Plot of the DPC methylene (H3-H11) NOEs to backbone H^{N} protons at pH 7.4 (black) and pH 4.0 (red). The plotted intensities have been scaled by the intensity of the H^{N} diagonal peak.

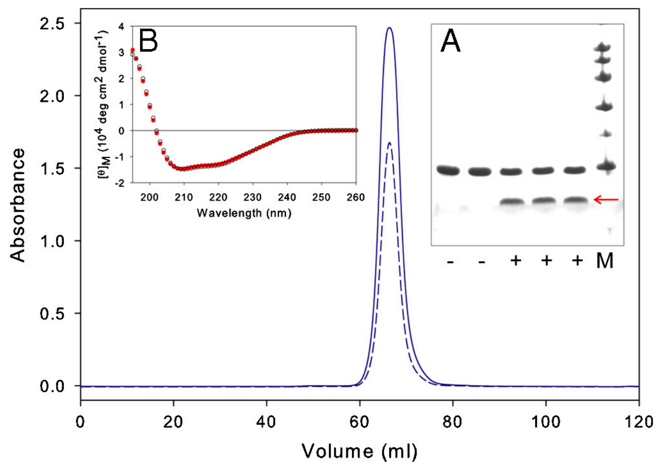

Fig. S6. Steps in the purification, and circular dichroism analysis of HAfp$^{1-23}$. Absorbance monitored at 280 nm (continuous blue) and 260 nm (dashed blue) for the fractionation of HAfp$^{1-23}$ on Superdex-75 column (1.6 × 60 cm, GE HealthCare, Piscataway, NJ) in 25 mM Tris-HCl, pH 7.4, 2 mM DPC. *Inset A*: *E. coli* expressed and Ni-NTA column purified 6H-GB1-FXa-HAfp fusion protein before and after cleavage with FXa protease shown in duplicate (–) and triplicate (+) lanes, respectively, analyzed by SDS-PAGE on 20% homogeneous PhastGel (GE Healthcare). The released HAfp$^{1-23}$ (red arrow) was separated away from the residual fusion protein by Ni-NTA affinity chromatography prior to the size-exclusion column on S-75 (shown by the blue UV traces). M denotes molecular weight markers in kD (97, 66, 45, 30, 20.1, and 14.4 from the top). *Inset B*: Nearly identical CD spectra of 43 μM HAfp$^{1-23}$ in 25 mM Tris-HCl, pH 7.3, 100 mM DPC (black) and 25 mM sodium formate, pH 3.9, 100 mM DPC (red), recorded at 32 °C.

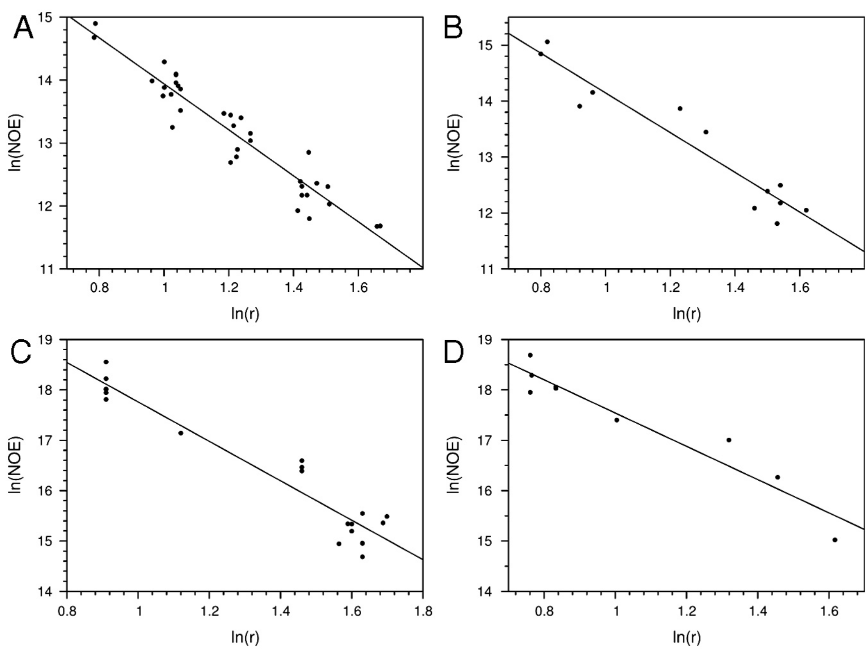

Fig. S7. NOE intensity vs. distance calibration plots for the (*A*, *B*) HNH-NOESY-HMQC three-dimensional (100 ms NOE mixing time) and the (*C*, *D*) NOESY two-dimensional (150 ms NOE mixing time) spectra of HAfp$^{1-23}$ at pH 7.4. The CH and CH_2 spin systems (*A*, *C*) were calibrated separately from CH_3 (*B*, *D*). Plotted is the natural logarithm of the NOE intensity against the natural logarithm of the interproton distance in an ideal helix. Two types of protons were included in the fit: (*i*) fixed distances for residues Phe^3 to Ile^{10}, which include backbone-backbone, backbone-Ala-H$^{\beta}$ and backbone-Ile-H$^{\gamma 2}$ distances, and (*ii*) distances between protons that are covalently linked in the Trp aromatic rings. The linear regression NOE exponent and correlation coefficient for the fits are: (*A*) $n = -3.65$, $R^2 = 0.91$, (*B*) $n = -3.55$, $R^2 = 0.91$, (*C*) $n = -3.91$, $R^2 = 0.92$, and (*D*) $n = -3.30$, $R^2 = 0.92$.

Table S1. Structural statistics for the 10 lowest energy structures of HAfp$^{1\text{–}23}$ at pH 7.4.

$Q_{\text{N-H}}$ *	8.3%
$Q_{\text{N-H}}$ †	10.0%
$Q^{\text{free}}_{\text{N-H}}$ *	21.4%
$Q^{\text{free}}_{\text{C}\alpha\text{-H}\alpha}$ *	22.9%
RDC tensor parameters	
$D_a(\text{NH})/R$ *	8.1 Hz/0.11
$D_a(\text{NH})/R$ †	−10.1 Hz/0.17
RMS deviation from experimental restraints (no. restraints)	
$^{1}\text{D}^{\text{NH}}$ (21) *	0.64 ± 0.03 Hz
$^{1}\text{D}^{\text{C}\alpha\text{H}\alpha}$ (26) *	2.59 ± 0.07 Hz
$^{2}\text{D}^{\text{H}\alpha2\text{-H}\alpha3}$ (3) *	3.5 ± 0.7 Hz
$^{1}\text{D}^{\text{C-(CH3)}}$ (6) *	0.45 ± 0.05 Hz
$^{1}\text{D}^{\text{NH}}$ (20) †	0.90 ± 0.07 Hz
$^{1}\text{D}^{\text{C'N}}$ (21) †	0.19 ± 0.01 Hz
$^{1}\text{D}^{\text{C'H}}$ (21) †	0.88 ± 0.02 Hz
$^{1}\text{D}^{\text{C}\alpha\text{C'}}$ (20) †	0.47 ± 0.02 Hz
Dihedral angles (40)	0.01 ± 0.02 deg
Short-range NOE (239)	0.028 ± 0.002 Å
Medium-range NOE (144)	0.030 ± 0.005 Å
Long-range NOE (66)	0.025 ± 0.004 Å
Deviations from idealized geometry	
Bonds	0.003 ± 0.00 Å
Angles	0.42 ± 0.01 deg
Impropers	0.33 ± 0.02 deg
Energy (kcal/mol)	
Total	48 ± 3
Bond	3.0 ± 0.5
Angle	16.0 ± 0.8
Improper	3.4 ± 0.5
van der Waals	12 ± 2
HBDB ‡	−32 ± 4
Dipolar	38 ± 1
NOE	8.8 ± 1.4
Dihedral	0.00 ± 0.00
Atomic RMS deviations§	
Backbone heavy atom (residues 1–23)	0.232 Å
Backbone heavy atom (residues 1–22)	0.109 Å
Side chain heavy atom (residues 1–23)	0.645 Å
Side chain heavy atom (residues 1–22)	0.626 Å
Ramachandran statistics ¶	
ϕ/ψ in most favored regions	99.3%
ϕ/ψ in additionally allowed regions	0.7%
ϕ/ψ in generously allowed regions	0.0%
Structure quality factors	
Molprobity Z-score (25)	0.19

*SAG-aligned sample. See the NMR Sample Preparation for details. Q and Q^{free} factors (26) were calculated using the denominator proposed by Clore et al. (27).
†d(GpG)-aligned sample. See the NMR Sample Preparation for details.
‡HBDB, the empirical hydrogen bond potential for Xplor-NIH (23).
§RMSD relative to the mean calculated for residues 1–23.
¶Evaluated using PROCHECK (28, 29).

Table S2. $^{3}J_{\text{NC}\gamma}$ and $^{3}J_{\text{C'C}\gamma}$ couplings that report on the χ^1 angles of Phe, Trp, and Tyr

Residue	$^{3}J_{\text{NC}\gamma}$ (Hz)	N-C$^{\alpha}$-C$^{\beta}$-C$^{\gamma}$ Dihedral	$^{3}J_{\text{COC}\gamma}$ (Hz)	C′-C$^{\alpha}$-C$^{\beta}$-C$^{\gamma}$ dihedral
Phe$^{3(\nu}$	1.4 ± 0.1	mixed	2.4 ± 0.1	mixed
Phe^{9}	2.7 ± 0.1	Trans	<1	gauche
Trp^{14}	2.2 ± 0.1	mostly trans	1.7 ± 0.1	mostly gauche
Trp^{21}	3.0 ± 0.1	trans	0.3 ± 0.6	gauche
Tyr^{22}	<1.1	gauche	3.5 ± 0.1	trans